Available online at www.sciencedirect.com
SCIENCE DIRECT
Journal of Power Sources 154 (2006) 290–297
JOURNAL OF POWER SOURCES
www.elsevier.com/locate/jpowsour

Crystallographic and electrochemical characteristics of $La_{0.7}Mg_{0.3}Ni_{3.5-x}(Al_{0.5}Mo_{0.5})_x$ ($x = 0$–0.8) hydrogen storage alloys

Xinbo Zhang [a], Danzi Sun [b], Wenya Yin [a], Yujun Chai [a], Minshou Zhao [a,*]

[a] *Graduate School of Chinese Academy of Sciences, Key Laboratory of Rare Earth Chemistry and Physics, Changchun Institute of Applied Chemistry, Chinese Academy of Sciences, Changchun 130022, PR China*
[b] *Graduate School of Chinese Academy of Sciences, State Key Laboratory of Electro-analytical Chemistry, Changchun Institute of Applied Chemistry, Chinese Academy of Sciences, Changchun 130022, PR China*

Received 17 November 2004; received in revised form 14 December 2004; accepted 25 March 2005
Available online 13 June 2005

Abstract

The crystal structure, hydrogen storage property and electrochemical characteristics of the $La_{0.7}Mg_{0.3}Ni_{3.5-x}(Al_{0.5}Mo_{0.5})_x$ ($x = 0$–0.8) alloys have been investigated systematically. It can be found that with X-ray powder diffraction and Rietveld analysis the alloys are of multiphase alloy and consisted of impurity LaNi phase and two main crystallographic phases, namely the La(La, Mg)$_2$Ni$_9$ phase and the $LaNi_5$ phase, and the lattice parameter and the cell volume of both the La(La, Mg)$_2$Ni$_9$ phase and the $LaNi_5$ phase increases with increasing Al and Mo content in the alloys. The *P–C* isotherms curves indicate that the hydrogen storage capacity of the alloy first increases and then decreases with increasing *x*, and the equilibrium pressure decreases with increasing *x*. The electrochemical measurements show that the maximum discharge capacity first increases from 354.2 ($x = 0$) to 397.6 mAh g^{-1} ($x = 0.6$) and then decreases to 370.4 mAh g^{-1} ($x = 0.8$). The high-rate dischargeability of the alloy electrode increases lineally from 55.7% ($x = 0$) to 73.8% ($x = 0.8$) at the discharge current density of 1200 mA g^{-1}. Moreover, the exchange current density of the alloy electrodes also increases monotonously with increasing *x*. The hydrogen diffusion coefficient in the alloy bulk increases with increasing Al and Mo content and thus enhances the low-temperature dischargeability of the alloy electrode.

Keywords: Structure characteristics; High-rate dischargeability; Low-temperature dischargeability; Exchange current density; Hydrogen diffusion coefficient

1. Introduction

Hydrogen storage alloy has attracted considerable attention in view of its potential as a new energy storage material. Recently, nickel-metal hydride battery (Ni-MH) in which a hydrogen storage alloy is employed as a negative electrode material has become a focus of interest as a candidate consumer-use battery by virtue of its several advantages: high reversible energy storage density, high resistance to overcharging and overdischarging, good charge–discharge kinetics, environmental compatibility and interchangeable with nickel-cadmium battery [1–6]. To date, almost all commercial Ni-MH batteries are employing AB_5-type alloys as negative electrode materials because of their good overall electrode properties [7]. However, the electrochemical capacity of the AB_5-type alloys is limited by the single $CaCu_5$-type hexagonal structure [8], the energy densities of the Ni-MH batteries are not competing favorably with some other advanced secondary batteries. Therefore, new type alloys with higher energy density, faster activation, better rate dischargeability and lower cost are urgently needed to replace the conventional rare earth-based AB_5-type alloys [9].

Fortunately, a new type of ternary alloys with the general formula of RMg_2Ni_9 (R: rare earth, Ca, Y) with $PuNi_3$-type structure have been found by Kadir et al. [10–12]. It is found that some of the R–Mg–Ni based ternary alloys can absorb–desorb 1.8–1.87 wt.% H_2 and are thus regarded as promising candidates for reversible gaseous hydrogen storage [13,14]. Whereafter, Chen et al. [6] have studied the

* Corresponding author. Tel.: +86 431 5262365.
E-mail address: eboat@ciac.jl.cn (M. Zhao).

0378-7753/$ – see front matter © 2005 Elsevier B.V. All rights reserved.
doi:10.1016/j.jpowsour.2005.03.217

structure and electrochemical characteristics of LaCaMg(Ni, M)$_9$ (M = Al, Mn) alloys, and almost at the same time, Kohno et al. [15] have reported that the discharge capacity of $La_{0.7}Mg_{0.3}Ni_{2.8}Co_{0.5}$ alloy reached 410 mAh g^{-1}. Unfortunately, the La–Mg–Ni–Co system hydrogen storage electrode alloys have some disadvantages, such as a high absorption–desorption plateau pressure, poor cyclic stability and so on [16]. In commercial AB_5–type alloys the presence of 10 wt.% of Co has indeed improved the cycling life of Ni-MH batteries. However, it influences negatively the discharge capacity as well as initial activation, and it constitutes about 40% of the material cost [17]. Much effort has been devoted to search for a more cost-effective substitute element with high reliability to improve the cycling life of Ni-MH batteries. It is believed that Al is one of the best candidates for cobalt substitution [18]. However, Al addition is detrimental to hydrogen diffusion from the alloy bulk to the surface and thus inevitably decreases the high-rate dischargeability of alloy electrode [2]. It is reported that Mo addition can remarkably improve the kinetic property [19]. Therefore, it can be expected that the overall electrochemical characteristics of the La–Mg–Ni–Co-type hydrogen storage alloys could be improved by substitution of Al and Mo for Ni in the alloys.

In this work, on the basis of our previous studies and the belief that the Al and Mo addition may result in some noticeable modification of the alloys, the structure and electrochemical characteristics of the $La_{0.7}Mg_{0.3}Ni_{3.5-x}(Al_{0.5}Mo_{0.5})_x$ (x = 0, 0.2, 0.4, 0.6, 0.8) hydrogen storage alloys have been investigated systematically.

2. Experimental details

2.1. Alloy preparation and X-ray diffraction analysis

All alloy samples were prepared by arc-melting carefully the constituent metals on a water-cooled copper hearth under argon atmosphere followed by annealing in vacuum for 100 h at 770 °C. The purity of the metals, i.e., La, Mg, Ni, Al and Mo is higher than 99.9 mass%. The samples were all inverted and remelted five times to ensure good homogeneity. A slight excess of Mg over composition was needed in order to compensate for evaporative loss of Mg under preparation conditions. Several attempts were done until the optimum preparative conditions were found. The final compounds were carefully checked by inductively coupled plasma-atomic emission spectrometry (ICP-AES) method using TJA Poems-type instrument. Thereafter, these alloy samples were mechanically crushed into fine powders of −300 mesh in mortar.

Crystallographic characteristics of the hydrogen storage alloys were investigated by X-ray diffraction on Rigaku D/Max 2500PC X-ray diffractometer (Cu Kα radiation, Bragg–Brentano geometry, 2θ range 10–100°, step size 0.02°, backscattered rear graphite monochromator) using JADE5 software [20]. The lattice constants and cell volume were calculated by RIETICA program after internal theta calibration using silicon as standard reference materials.

2.2. Electrochemical measurement

The preparation of the disk-type electrodes, the setup of the electrochemical cell and the test of electrochemical properties were similar as described in our previous paper [21].

Pressure–composition isotherms (*P–C–T*) curves were electrochemically obtained by converting the equilibrium potential of the metal hydride electrode to the equilibrium pressure of hydrogen on the basis of Nernst equation using electrochemical data [22] as reported in Ref. [23]. The equilibrium potential curves were obtained by alternating the following two processes: (1) a pulse discharge of (25 mA g^{-1} × 0.25 h) and (2) a rest period until the potential became almost constant.

Linear polarization curves were performed on a EG&G PARC's Model 273 Potentiostat/Galvanostat station by scanning the electrode potential at the rate of 0.1 mV s^{-1} from −5 to 5 mV (versus open circuit potential) at 50% depth of discharge at 298 and 233 K, respectively. The exchange current density I_0 was calculated from the slopes of polarization curves by the following equation [18]:

$$I_0 = \frac{RT}{FR_p}$$

where R, T and F have their general meanings. The potential step experiments were performed on the same instrument (using the M352 CorrWare electrochemical/corrosion software) at 100% charge state. A +500 mV potential was applied and the discharge time was 500 s.

3. Results and discussion

3.1. Alloy composition and structure characteristic

It is well known that the low melting Mg metal will be inevitably lost during the sample preparation by arc melting. We have tried many ways to overcome this problem, such as using Mg–Ni master alloy as an Mg additive, decreasing the melting current, adding a slight excess of Mg over sample composition and so on. Among all these methods, we found that the third one is the most effective ways to compensate evaporative loss of Mg. Several attempts had been done until the optimum preparative conditions were found. In this paper, the lost weight during sample preparation is almost the same as excess Mg added. The results of ICP-AES analysis for all compounds are given in Table 1. It can be seen that the final composition of all the alloys is identical with the original composition.

The crystal structures of the $La_{0.7}Mg_{0.3}Ni_{3.5-x}(Al_{0.5}Mo_{0.5})_x$ (x = 0–0.8) alloy have been identified and refined by means of X-ray powder diffraction data. Fig. 1 shows the Rietveld refinement pattern of the XRD profiles

Table 1
Composition of the $La_{0.7}Mg_{0.3}Ni_{3.5-x}(Al_{0.5}Mo_{0.5})_x$ (x = 0–0.8) alloys

Sample	La (mg g^{-1})	Mg (mg g^{-1})	Ni (mg g^{-1})	Al (mg g^{-1})	Co (mg g^{-1})	La:Mg:Ni:Al:Mo[a]
x = 0.0	313.69	23.53	662.78	0	0	2.26:0.97:11.29:0:0
x = 0.2	313.13	23.49	623.80	8.69	30.90	2.25:0.97:10.63:0.32:0.32
x = 0.4	312.57	23.44	584.95	17.35	61.68	2.25:0.96:9.97:0.64:0.64
x = 0.6	312.02	23.40	546.25	25.97	92.36	2.25:0.96:9.31:0.96:0.96
x = 0.8	311.47	23.36	507.67	34.57	122.93	2.24:0.96:8.65:1.28:1.28

[a] Atomic ratio.

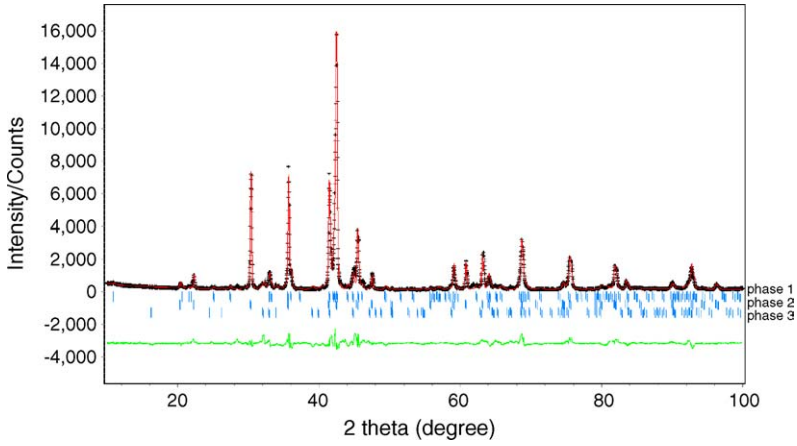

Fig. 1. Rietveld refinement pattern of the XRD profiles for the $La_{0.7}Mg_{0.3}Ni_{3.3}(Al_{0.5}Mo_{0.5})_{0.2}$ hydrogen storage alloy (phase 1, La(La, Mg)$_2$Ni$_9$; phase 2, $LaNi_5$; phase 3, LaNi).

for $La_{0.7}Mg_{0.3}Ni_{3.3}(Al_{0.5}Mo_{0.5})_{0.2}$ alloy as a representative example of $La_{0.7}Mg_{0.3}Ni_{3.5-x}(Al_{0.5}Mo_{0.5})_x$ (x = 0–0.8) hydrogen storage alloys. The final crystallographic parameter of the pseudo-La_2MgNi_9 phase (Ni is partially substituted by Al and Mo) and pseudo-$LaNi_5$ phase (Ni is partially substituted by Al and Mo) is tabulated in Tables 2 and 3, respectively. It can be seen that the substitution of Al and Mo for Ni still retain the rhombohedral $PuNi_3$-type structure and the hexagonal $CaCu_5$-type structure, respectively. This phenomenon is consistent with the result in Liao et al.'s paper [16]. For convenience of discussing, in this work La(La, Mg)$_2$Ni$_9$ phase and $LaNi_5$ phase are employed to represent the pseudo-La_2MgNi_9 phase and pseudo-$LaNi_5$, respectively. The lattice parameter, cell volume, and phase abundance of the $La_{0.7}Mg_{0.3}Ni_{3.5-x}(Al_{0.5}Mo_{0.5})_x$ (x = 0–0.8) alloys are presented in Table 4. We can find that all the alloys consist of impurity LaNi phase and two main crystallographic phases, namely the La(La, Mg)$_2$Ni$_9$ phase and the $LaNi_5$ phase. Fig. 2 shows the lattice parameters and unit cell volume of the alloys as a function of x. It can be seen that a and c parameters of both the La(La, Mg)$_2$Ni$_9$ phase and the $LaNi_5$ phase in the alloys all increase linearly with the increase of x, which is mainly attributed to the fact that the atomic radius of Al (1.432 Å) and Mo (1.363 Å) is larger than that of Ni (1.246 Å), respectively.

Table 2
Crystallographic parameter for pseudo-La_2MgNi_9 by using X-ray diffraction Cu Kα (λ = 1.5405981 Å) at 298 K in a space group R-3m and Z = 3[a]

Atom	Site	Metal atom position			Occupancy
		x	y	z	
La1	3a	0	0	0	1
La2	6c	0	0	0.1448(1)	0.463
Mg1	6c	0	0	0.1448(1)	0.537
Ni1	6c	0.3288(2)	0	0.3288(2)	0.891
Ni2	3b	0.5	0	0.5	0.912
Ni3	18h	0.0843(3)	0.5028(1)	0.0843(3)	0.934
Al1	6c	0.3288(2)	0	0.3288(2)	0.036
Al2	3b	0.5	0	0.5	0.045
Al3	18h	0.0843(3)	0.5028(1)	0.0843(3)	0.054
Mo1	6c	0.3288(2)	0	0.3288(2)	0.073
Mo2	3b	0.5	0	0.5	0.043
Mo3	18h	0.0843(3)	0.5028(1)	0.0843(3)	0.012

[a] Structure was refined by using the Rietveld refinement program Rietica. The pattern factor R_p = 6.7, the weighted pattern factor R_{wp} =9.0 and the goodness of fit GoF = 2.5.

Table 3
Crystallographic parameter for pseudo-$LaNi_5$ by using X-ray diffraction Cu Kα (λ = 1.5405981 Å) at 298 K in a space group $P6/mmm$ and Z = 1[a]

Atom	Site	Metal atom position			Occupancy
		x	y	z	
La1	1a	0	0	0	1
Ni1	2c	0.3333	0.6667	0	0.673
Ni2	3g	0.5	0	0.5	0.684
Al1	2c	0.3333	0.6667	0	0.152
Al2	3g	0.5	0	0.5	0.192
Mo1	2c	0.3333	0.6667	0	0.175
Mo2	3g	0.5	0	0.5	0.124

[a] Structure was refined by using the Rietveld refinement program Rietica. The pattern factor R_p = 6.3, the weighted pattern factor R_{wp} = 8.2 and the goodness of fit GoF = 2.1.

Table 4
Characteristics of alloy phases in $La_{0.7}Mg_{0.3}Ni_{3.5-x}(Al_{0.5}Mo_{0.5})_x$ (x = 0–0.8) alloys

Sample	Phase	Phase abundance (wt.%)	Lattice parameter (Å)			Cell volume (Å)
			a	*b*	*c*	
x = 0.0	La(La, Mg)$_2$Ni$_9$	80.23	5.040		24.339	535.42
	LaNi$_5$	19.53	5.115		4.066	92.13
	LaNi	0.24	3.909	10.945	4.542	194.32
x = 0.2	La(La, Mg)$_2$Ni$_9$	75.41	5.064		24.618	546.73
	LaNi$_5$	24.33	5.125		4.083	92.87
	LaNi	0.26	3.910	10.951	4.543	194.52
x = 0.4	La(La, Mg)$_2$Ni$_9$	68.73	5.095		24.660	554.39
	LaNi$_5$	31.06	5.130		4.086	93.12
	LaNi	0.21	3.911	10.956	4.544	194.71
x = 0.6	La(La, Mg)$_2$Ni$_9$	67.01	5.129		24.874	566.69
	LaNi$_5$	32.97	5.143		4.112	94.19
	LaNi	0.02	3.912	10.963	4.541	194.75
x = 0.8	La(La, Mg)$_2$Ni$_9$	60.96	5.177		24.966	579.48
	LaNi$_5$	38.72	5.149		4.120	94.6
	LaNi	0.32	3.913	10.964	4.543	194.9

Fig. 3 shows the abundances of the La(La, Mg)$_2$Ni$_9$ phase and the LaNi$_5$ phase as a function of x in the alloys. As can be seen in Fig. 3 and Table 4, the La(La, Mg)$_2$Ni$_9$ phase abundance decreases from 80.23% to 60.96% with increasing of x, however, the LaNi$_5$ phase abundance increases from 19.53% to 38.72%. These results may influence the electrochemical characteristics of the alloy studied.

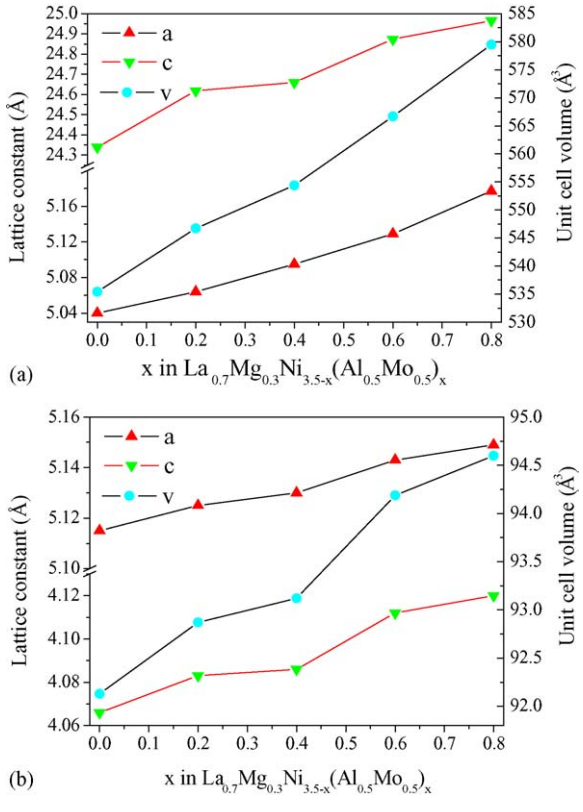

Fig. 2. Variations of the cell parameters and volumes as the function of x in $La_{0.7}Mg_{0.3}Ni_{3.5-x}(Al_{0.5}Mo_{0.5})_x$ alloys (x = 0–0.8): (a) La(La, Mg)$_2$Ni$_9$ phase; (b) LaNi$_5$ phase.

3.2. P–C isotherms

The electrochemical pressure–composition isotherms method is very useful for examining the charging and discharging levels of hydrogen in an anode, although the calculated pressures pertain to a quasi-equilibrium state [18]. Fig. 4 shows the electrochemical P–C isotherms for $La_{0.7}Mg_{0.3}Ni_{3.5-x}(Al_{0.5}Mo_{0.5})_x$ (x = 0, 0.2, 0.4, 0.6, 0.8) alloy electrodes at 298 K. It can be seen that the desorption pressure reduces continually as the Al and Mo additions increase. This means that the stability of the hydrides of alloys increases with increasing Al and Mo content because of the larger unit cell volume of the alloy. The phenomenon observed here is consistent with those reported previously for AB_3 alloys [14] and most AB_5 alloys [24]. Moreover, it can

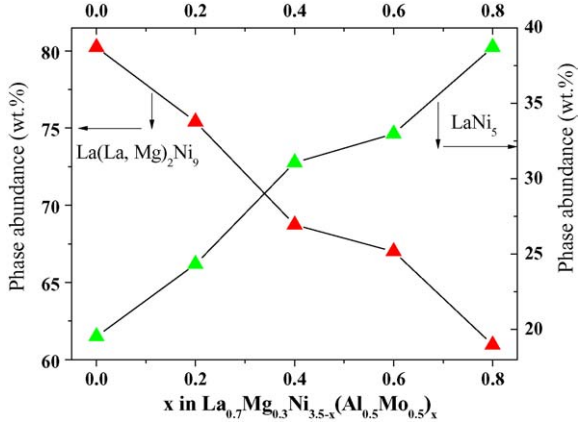

Fig. 3. Phase abundance of the La(La, Mg)$_2$Ni$_9$ phase and the LaNi5 phase existing in the $La_{0.7}Mg_{0.3-x}(Al_{0.5}Mo_{0.5})_x$ (x = 0–0.8) alloys.

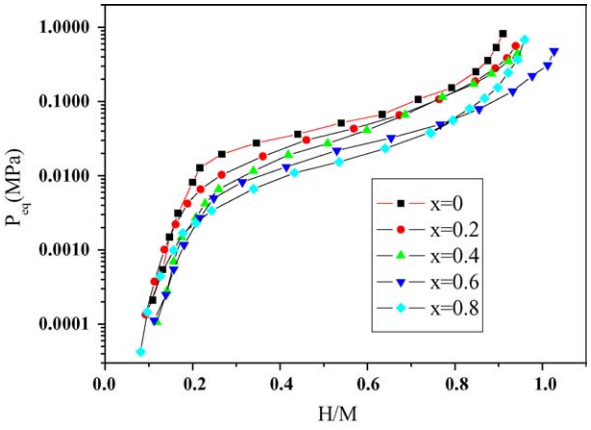

Fig. 4. The electrochemical desorption *P–C–T* curves for $La_{0.7}Mg_{0.3}Ni_{3.5-x}(Al_{0.5}Mo_{0.5})$ (x = 0, 0.2, 0.4, 0.6, 0.8) alloys at 298 K.

be seen that there is only one plateau in each *P–C–T* curve as shown in Fig. 4. Since the unit cell of the AB_3 compounds contains one-third AB_5 structure and two-thirds AB_2 structure [6], it is possible that the plateau pressure of the La(La, Mg)$_2$Ni$_9$ phase is similar to that of the $LaNi_5$ phase or the difference between their plateau pressures is too small to be observed.

With the increase of Al and Mo contents in the alloys, the hydrogen storage capacity first increases from 0.910 to 1.027, and then decreases to 0.959. This may be due to causes described as follows: As mentioned above, the plateau pressure decreases with increase of Al and Mo addition in the alloys, which enhances the intrinsic hydrogen storage capacity of the alloys. However, Sakai et al. [2,18] pointed out that the formation of passive layer of $Al(OH)_3$ inevitably decreases the hydrogen storage capacity, because such a layer not only weakens the surface electrocatalytic activity and prevents the diffusion of hydrogen into or from the alloy bulk, but also decreases the content of hydrogen absorption elements La and Mg in the alloys and thus reduces hydrogen storage capacity of the alloy. On the other hand, it is reported that the addition of Mo to the alloy leads to the improvement of the electrocatalytic activity on the alloy surface [19]. Therefore, it is reasonable to assume that, with Al and Mo content addition of lower than a certain amount, the positive effect is dominant and will cause an increase in the hydrogen storage capacity. However, when Al and Mo content exceed the critical content, the negative effect will become dominant and give rise to a decrease in the specific capacity. Overall, the combined effect of the above factors will inevitably result in an optimal value for the hydrogen storage capacity. The recommended amount of Al and Mo addition is x = 0.6 from our work.

3.3. Discharge performance

The cyclic numbers needed to activate the electrodes and the maximum discharge capacity of the $La_{0.7}Mg_{0.3}Ni_{3.5-x}(Al_{0.5}Mo_{0.5})_x$ (x = 0–0.8) alloy electrodes are listed in Table 5. It can be seen that all these alloys can be easily activated to reach the maximum capacity within two cycles. For the alloys with composition range of x = 0–0.8, the maximum discharge capacity C_{max} improves significantly with the increase in x and reaches a maximum at x = 0.6, and then decreases as x increases further. The variation of maximum discharge capacity of the alloys is essentially consistent with the variation of the H/M in the alloys. The maximum discharge capacity of the $La_{0.7}Mg_{0.3}Ni_{2.9}(Al_{0.5}Mo_{0.5})_{0.6}$ alloy electrodes is 397.6 mAh g^{-1}, which is noticeably higher than that of the commercial AB_5-type alloys.

Table 5
Electrode performance of $La_{0.7}Mg_{0.3}Ni_{3.5-x}(Al_{0.5}Mo_{0.5})_x$ (x = 0–0.8) alloy electrodes

Sample	H/M	C_{max} (mAh g^{-1})	N_a[a]	HRD_{1200}[b] (%)	S_{70} (%)
x = 0.0	0.910	354.2	2	55.7	54.2
x = 0.2	0.939	364.6	2	58.8	61.3
x = 0.4	0.979	379.7	1	63.5	66.6
x = 0.6	1.027	397.6	1	70.5	70.8
x = 0.8	0.959	370.4	1	73.8	75.7

[a] The cycle numbers needed to activate the electrodes.
[b] The high-rate dischargeability at the discharge current density of 1200 mA g^{-1}.

Fig. 5 shows the discharge curves (the fifth cycle) of the alloy electrodes. Obviously, each curve has a wide discharge potential plateau based on the oxidation of desorbed hydrogen from the hydride. Besides, the discharge plateau shifts towards a more positive potential as Al and Mo addition increases in the alloys. As shown in Fig. 5, the middle-discharge potential (potential at 50% depth of discharge) decreases from −0.8707 to −0.818 V in agreement with the reduction of desorption plateau pressure when x increases from 0 to 0.8 in the alloys.

3.4. Cyclic stability

The cycling capacity retention rate, expressed as S_{70} (%) = $C_{70}/C_{max} \times 100$ (where C_{max} is the maximum

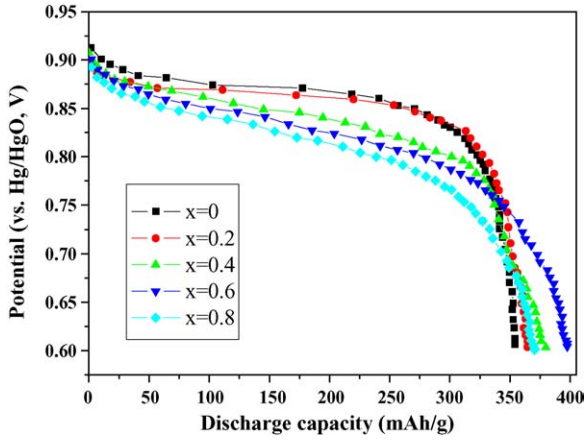

Fig. 5. The discharge curves of $La_{0.7}Mg_{0.3}Ni_{3.5-x}(Al_{0.5}Mo_{0.5})_x$ (x = 0–0.08) alloy electrodes at the discharge current density of 60 mA g^{-1} and 298 K.

discharge capacity, C_{70} is the discharge capacity at the 70th cycles), is also listed in Table 5 after 70 cycles at discharge current of 60 mA g^{-1}. As seen in Table 5, the capacity retention rate (S_{70}) increases noticeably from 54.2% to 75.7% with x increasing from 0 to 0.8, indicating that the cyclic stability of the La–Mg–Ni–Al–Mo system alloys is improved markedly with the increase of Al and Mo content in the alloys. It is known that the capacity degradation of La–Mg–Ni-type alloy electrode results primarily from two factors, the corrosion of Mg and La elements and the pulverization of the alloy particles [24]. The Al substitution results in the formation of the protective oxide (hydroxide) of Al on the alloy surface and a subsequent strong protection to the alloy from further corrosion of La and Mg.

3.5. High-rate dischargeability (HRD) and electrochemical kinetics

As an important kinetics property of the hydride electrode in battery, it is very important to hold back the decrease of the discharge capacity even at the high charge–discharge current density. Fig. 6 shows the relationship between the high-rate dischargeability and the discharge current density of the $La_{0.7}Mg_{0.3}Ni_{3.5-x}(Al_{0.5}Mo_{0.5})_x$ (x = 0–0.8) alloy electrodes. The HRD of the alloy electrodes for the discharge current density of 1200 mA g^{-1} are also listed in Table 5. It can be seen that as x increases, the HRD of the alloy electrodes increases from 55.7% (x = 0) to 73.8% (x = 0.8). It is well known that the HRD of metal hydride electrode are mainly influenced by the electrochemical reaction kinetics on the alloy powder surface and the diffusion rate of hydrogen in the bulk of the alloy [25]. To examine the effect of the partial substitution of Al and Mo for Ni on the discharge kinetics, linear polarization was preformed on these alloy electrodes. Based on the measured linear polarization curves, values of exchange current density I_0 were evaluated for the alloy electrodes and are summarized in Table 6. It can be seen that the I_0 increases monotonically with increasing Al and Mo content in the alloys. This may be attributed to the reasons as follows; Iwakura et al. [19] pointed out that the addition of Mo to the alloy leads to the improvement of the electrocatalytic activity on the alloy surface. Moreover, perhaps there is a metallic Ni/Mo work with higher activity on the alloy surface [26]. Overall, due to increase of Mo content in the alloy, the concentration of the Mo on the alloy surface increases and thus increases the I_0 of the alloy electrodes. Further investigations in this aspect are going on in our group. Fig. 7 shows high-rate dischargeability as a function of the I_0 for the hydrogen evolution reaction at the alloy electrodes. It is found that the HRD is a linear function of I_0, while the hydrogen diffusion coefficient maintains almost unchanged (11.6–12.3 × 10^{-10} cm^2 s^{-1}). Iwakura et al. [19] have pointed out that if the electrochemical reaction on the surface is a rate-determining factor, a linear dependence of the high-rate dischargeability on the exchange current density should be observed. In contrast if the diffusion of hydrogen in the alloy bulk is a rate-determining factor, the high-rate dischargeability should be constant, irrespective of exchange current density. Therefore, in the present study, the HRD is essentially controlled by the charge-transfer reaction of hydrogen on the surface at a discharge current density of 1200 mAh g^{-1}.

Table 6
Electrochemical kinetic parameters of $La_{0.7}Mg_{0.3}Ni_{3.5-x}(Al_{0.5}Mo_{0.5})_x$ (x = 0–0.8) alloy electrodes

Sample	Exchange current density, I_0 (mA g^{-1})		Hydrogen diffusion coefficient, D ($\times 10^{-10}$ cm^2 s^{-1})	
	298 K	233 K	298 K	233 K
x = 0.0	205.42	53.42	11.6	1.4
x = 0.2	208.26	53.56	11.7	2.6
x = 0.4	226.33	53.98	11.7	3.2
x = 0.6	237.14	54.12	12.1	4.2
x = 0.8	240.12	54.63	12.3	5.4

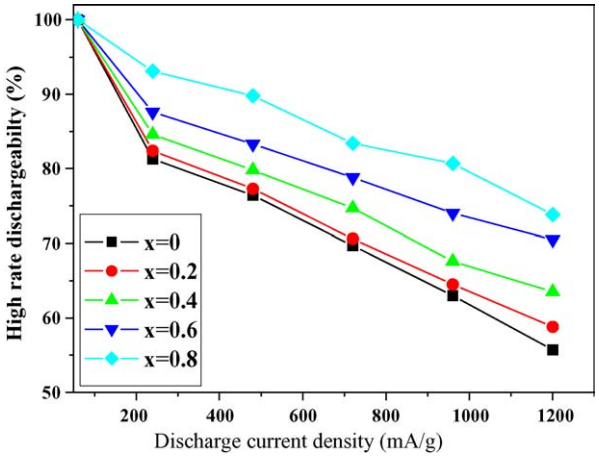

Fig. 6. The high-rate dischargeability (HRD) of the $La_{0.7}Mg_{0.3}Ni_{3.5-x}(Al_{0.5}Mo_{0.5})_x$ (x = 0, 0.2, 0.4, 0.6, 0.8) alloy electrodes at 298 K.

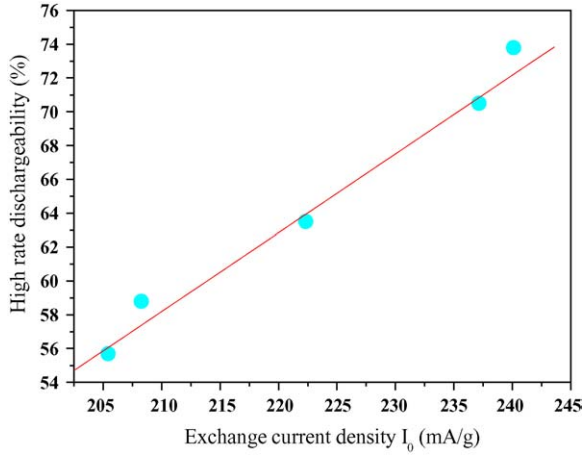

Fig. 7. High-rate dischargeability as a function of exchange current density for hydrogen evolution of $La_{0.7}Mg_{0.3}Ni_{3.5-x}(Al_{0.5}Mo_{0.5})$ (x = 0–0.8) alloy electrodes.

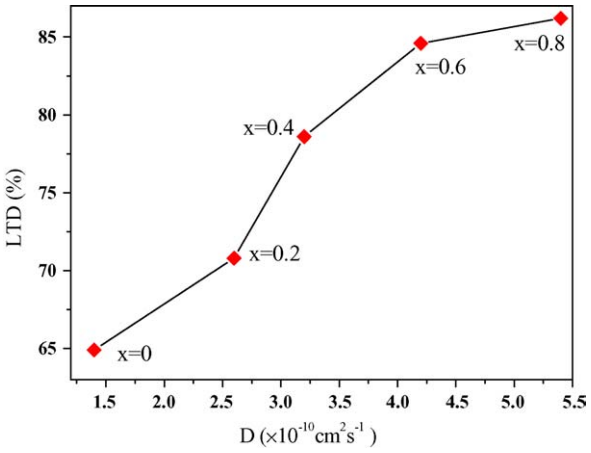

Fig. 8. The low-temperature dischargeability (LTD) as a function of hydrogen diffusion coefficient (D) of the $La_{0.7}Mg_{0.3}Ni_{3.5-x}(Al0.5Mo0.5)_x$) ($x$ = 0, 0.2, 0.4, 0.6, 0.8) alloy electrodes at 233 K.

3.6. Low-temperature dischargeability (LTD)

It has been reported that the discharge capacity of the negative electrode in nickel-metal hydride decrease drastically with decreasing temperature [27–29]. Sakai et al. [2] pointed out that the dischargeability of the negative electrodes at relatively low temperature depended on the hydrogen diffusion and/or charge-transfer process occurring at the metal electrolyte interface. The hydrogen diffusion coefficient D of hydrogen in the alloy bulk is evaluated using the method described by Iwakura et al. [19]. The low-temperature dischargeability, expressed as LTD_{233} (%) = $C_{233}/C_{298} \times 100$ (where C_{233} and C_{298} are the discharge capacity at 233 and 298 K, respectively). Fig. 8 shows the LTD as a function of D in the alloy electrodes. It can be that the LTD increases with increasing D. The D of the $La_{0.7}Mg_{0.3}Ni_{3.5-x}(Al_{0.5}Mo_{0.5})_x$ (x = 0, 0.2, 0.4, 0.6, 0.8) alloy electrodes at 233 K are also listed in Table 6, respectively. It can be found that the I_0 maintain almost unchanged (53.42–54.63 mA g^{-1}); however, the D increases remarkably with increasing x, which implies that the hydrogen diffusion in alloy bulk probably becomes the rate-determining factor for low-temperature dischargeability at 233 K. In general, the cell volume expansion results in the stability of hydride (decrease of ΔH), leading to the decrease of D value [27]. However, the D value increases with increasing of x (increasing of the unit cell volume) in present work, which can be attributed to the change in the relative amounts of La(La, $Mg)_2Ni_9$ phase and $LaNi_5$ phase owing to Al and Mo substitution. As mentioned above, the La(La, $Mg)_2Ni_9$ phase abundance decreases from 80.23% to 60.96% with increasing of x, however, the $LaNi_5$ phase abundance increases from 19.53% to 38.72%. These results may result more phase boundary, which will provide path for hydrogen diffusion and thus increase the D. Zhao and Sun thought [29] that desorption of hydrogen in metal hydride is an endothermal reaction and may be a rate-limiting step during the discharge process of metal hydride at relatively low temperature (for example, at 233 K).

4. Conclusion

The effect of Al and Mo substitution for Ni on the structure, hydrogen storage characteristics and electrochemical properties of the $La_{0.7}Mg_{0.3}Ni_{3.5-x}(Al_{0.5}Mo_{0.5})_x$ (x = 0–0.8) hydrogen storage alloys have been investigated systematically. The results of X-ray powder diffraction and Rietveld analysis show that the alloys are all consisted of the La(La, $Mg)_2Ni_9$ phase and the $LaNi_5$ phase, and the lattice parameter and cell volume of both the La(La, $Mg)_2Ni_9$ phase and the $LaNi_5$ phase increase with increasing Al and Mo content. The P–C isotherms reveal that the hydrogen storage capacity increases to a maximum and then decreases with increasing x, but the plateau pressure decreases continuously with increasing x. The electrochemical measurements show that the maximum discharge capacity increases first when x increases from 0.0 (354.2 mAh g^{-1}) to 0.6 (397.6 mAh g^{-1}) and then decreases when x reaches 0.8 (370.4 mAh g^{-1}). For the discharge current density of 1200 mA g^{-1}, the high-rate dischargeability of the alloy electrodes increases lineally from 54.2% (x = 0) to 75.7% (x = 0.8) due to the increase of the exchange current density at 298 K. The hydrogen diffusion coefficient D increases with increasing Al and Mo content, and thus increases the low-temperature dischargeability LTD of the alloy electrodes.

Acknowledgement

This work was financially supported by the National Natural Science Foundation of China (Grant No. 20171042).

References

[1] J.J.G. Willems, K.H.J. Buschow, J. Less-Common Met. 129 (1987) 13.
[2] T. Sakai, H. Miyamura, N. Kuriyama, A. Kato, K. Oguro, H. Ishikawa, J. Electrochem. Soc. 137 (1990) 795.
[3] T. Kohno, H. Yoshida, F. Kawashima, T. Inaba, I. Sakai, M. Yamamoto, M. Kanda, J. Alloys Compd. 311 (2000) 5.
[4] J.J.G. Willems, Philips J. Res. 39 (Suppl. 1) (1984) 1.
[5] H.G. Pan, Y.F. Zhu, M.X. Gao, Q.D. Wang, J. Electrochem. Soc. 149 (2002) 829.
[6] J. Chen, N. Kuriyama, H.T. Takeshita, H. Tanaka, T. Sakai, M. Haruta, Electrochem. Solid-State Lett. 3 (6) (2000) 249.
[7] T. Sakai, I. Uehara, H. Ishikawa, J. Alloys Compd. 293–295 (1999) 762.
[8] J.J. Reilly, G.D. Adzic, J.R. Johnson, T. Vogt, S. Mukerjee, J. McBreen, J. Alloys Compd. 293–295 (1999) 569.
[9] Y.F. Liu, H.G. pan, Y.F. Zhu, R. Li, Y.Q. Lei, Mater. Sci. Eng. A. 372 (2004) 163.
[10] K. Kadir, T. Sakai, I. Uahara, J. Alloys Compd. 257 (1997) 115.
[11] K. Kadir, N. Kuriyama, T. Sakai, I. Uehara, L. Eriksson, J. Alloys Compd. 284 (1999) 145.

[12] K. Kadir, T. Sakai, I. Uahara, J. Alloys Compd. 287 (1999) 264.
[13] K. Kadir, T. Sakai, I. Uahara, J. Alloys Compd. 302 (2000) 112.
[14] J. Chen, H.T. Takeshita, H. Tanaka, N. Kuriyama, T. Sakai, J. Alloys Compd. 302 (2000) 304.
[15] T. Kohno, H. Yoshida, F. Kawashima, T. Inaba, I. Sakai, M. Yamamoto, M. Kanda, J. Alloys Compd. 311 (2000) 5.
[16] B. Liao, Y.Q. Lei, L.X. Chen, G.L. Lu, H.G. Pan, Q.D. Wang, J. Power Sources 129 (2004) 358.
[17] P.H. Notton, P. Hokkeling, J. Electrochem. Soc. 138 (1991) 1877.
[18] T. Sakai, H. Miyamura, N. Kuriyama, A. Kato, K. Oguro, H. Ishikawa, J. Less-Common Met. 159 (1990) 127.
[19] C. Iwakura, H. Senoh, K. Morimoto, Y. Hara, H. Inoue, Electrochem. 70 (1) (2002) 2.
[20] Materials Data JADE Release 5, XRD Pattern Processing, Materials Data Inc. (MDI), 1997.
[21] X.B. Zhang, Y.J. Chai, W.Y. Yin, M.S. Zhao, J. Solid State Chem. 177 (2004) 2373.
[22] J. Balej, Int. J. Hydrogen Energy 10 (1985) 365.
[23] C. Iwakura, T. Asaoka, H. Yoneyama, T. Sakai, K. Oguro, H. Ishikawa, Nippon Kagaku Kaishi (1988) 1482.
[24] H.G. Pan, Q.W. Jin, M.X. Gao, Y.F. Liu, R. Li, Y.Q. Lei, J. Alloys Compd. 373 (2004) 237.
[25] H.G. Pan, Y.F. Liu, M.X. Gao, Y.Q. Lei, Q.D. Wang, J. Electrochem. Soc. 150 (5) (2003) 565.
[26] M.T. Yeh, V.M. Beibutian, S.E. Hsu, J. Alloys Compd. 293–295 (1999) 721.
[27] C. Iwakura, T. Oura, H. Inoue, M. Matsuoka, Electrochim. Acta 41 (1996) 117.
[28] H. Senoh, Y. Hara, H. Inoue, C. Iwakura, Electrochim. Acta 46 (2001) 967.
[29] M. Zhao, C. Sun, Hydrogen materials science and chemistry of metal hydrides, in: T. Nejet Vezirogle, et al. (Eds.), II Materials, Physics and Chemistry, vol. 82, Kluwer Academic Publisher, 2002, pp. 29–34.